INTERNATIONAL JOURNAL OF HYDROGEN ENERGY 48 (2023) 35753–35764

Available online at www.sciencedirect.com

ScienceDirect

journal homepage: www.elsevier.com/locate/he

Molybdenum-containing carbon nanofiber supported palladium catalyst for formic acid oxidation reaction

*Fahimah Abd Lah Halim, Yugo Osaka, Akio Kodama, Takuya Tsujiguchi**

Faculty of Mechanical Engineering, Institute of Science and Engineering, Kanazawa University, Kakumamachi, Kanazawa, Ishikawa, 920-1192, Japan

HIGHLIGHTS

- Molybdenum-containing carbon nanofiber supported Pd catalyst was synthesized.
- Pd/MoS-VECNF catalysts were tested for formic acid oxidation.
- Formic acid oxidation activity is improved by the addition of molybdenum.
- Superior stability is achieved by the molybdenum-containing catalyst.
- Pd/MoS-VECNF catalyst is promising for direct formic acid fuel cells application.

ARTICLE INFO

Article history:
Received 18 February 2023
Received in revised form
16 May 2023
Accepted 1 June 2023
Available online 16 June 2023

Keywords:
Formic acid oxidation reaction
Carbon nanofiber
Pd-based catalyst
Direct formic acid fuel cell

ABSTRACT

Numerous studies have reported the development of Pd-based catalyst for the anode direct formic acid fuel cell (DFAFC) that improves the electrocatalytic activities. We have now developed a carbon nanofiber embedded with carbon black (Vulcan) and molybdenum sulfide (MoS_2) nanoparticles as the Pd support for the FAOR catalyst. The MoS_2-Vulcan embedded carbon nanofiber (MoS-VECNF) was first prepared by electrospinning and heat treatment. The MoS-VECNF was prepared with different weight ratios of MoS_2 to polyacrylonitrile (PAN). The prepared support was then loaded with 20 wt% Pd nanoparticles by the polyol method. The Pd/MoS-VECNF catalyst demonstrated a better FAOR activity and stability as compared to the Pd/VECNF catalyst with 0.10 as the optimum weight ratio. The achieved peak current density was 1.46 times higher than that of the Pd/VECNF catalyst. The presence of MoS_2 nanoparticles in the carbon support produced a strong metal-support interaction which improved the FAOR activity and stability of the catalyst. Therefore, the Pd/MoS-VECNF catalyst is suggested to be promising for DFAFC applications.

Introduction

Direct formic acid fuel cells (DFAFCs) are some of the polymer electrolyte membrane fuel cells (PEFCs) types that have gained much attention due to their high theoretical voltage (1.48 V), low formic acid toxicity, low fuel crossover, low operating temperature and ease of fuel transport and storage. These advantages allow the DFAFC to be used as the power source for portable devices such as cell phones and laptops. Moreover, formic acid is also a promising hydrogen energy carrier which means that it can be used as the hydrogen source for

* *Corresponding author.*
E-mail address: tsujiguchi@se.kanazawa-u.ac.jp (T. Tsujiguchi).
https://doi.org/10.1016/j.ijhydene.2023.06.004

the hydrogen-PEFC [1]. However, in the case of the DFAFC operation, the power output is still low due to the poor performance of the anode catalyst at which the formic acid oxidation reaction (FAOR) takes place. The FAOR can proceed via two routes which are the direct and indirect pathway reactions. The direct pathway involving reactive intermediate species (HCOO) and produces CO_2. Meanwhile, the indirect pathway is an incomplete formic acid oxidation that produces CO as shown by the following reaction. The strongly adsorbed CO is considered a poison blocking the catalyst surface that inhibits further oxidation of the formic acid. Thus, the direct pathway is highly desirable for the formic acid oxidation [2].

$$\text{Directpathway}: HCOOH \rightarrow HCOO_{ads} \rightarrow CO_2 + 2H^+ + 2e^- \quad (1)$$

$$\text{Indirect pathway}: HCOOH \rightarrow HCOO_{ads} \rightarrow CO_{ads} + H_2O \rightarrow CO_2 + 2H^+ + 2e^- \quad (2)$$

Pd and Pt catalysts are commonly used for the formic acid oxidation, but Pd is shown to be more active than Pt thus preferable for the direct pathway reaction and excellent anti–CO–poisoning capacity [3–5]. However, the development of a highly active and stable Pd catalyst is still challenging due to the adsorption of reaction intermediates on the Pd surface and Pd dissolution [6].

A vast number of studies has introduced effective strategies for improving the FAOR activity of the Pd catalyst. One of the strategies is alloying the Pd with other non-noble metals, such as Cu, Co, Ni, Ru, Sn, Bi, Ir, Cr, Au or Ag. These metals are added to Pd and form bimetallic [7–15] or trimetallic [16–19] catalysts. The addition of these metals caused a weaker adsorption of CO on the catalyst surface as compared to when Pd alone is used as the catalyst, hence, it promotes the electrocatalytic activity [5,10]. In recent study, improved FAOR activity was also demonstrated by the Ga-modified PdAgCo/CNT catalyst. Addition of a fourth metal to the catalyst reduces the catalyst particle size, resulting in an increased active surface area [20]. Modification of the support material is reported as another effective way for promoting the electrocatalytic activity of the Pd catalyst. Carbonaceous materials, such as carbon black, carbon nanotubes, carbon nanofibers and graphene, are common supports for the Pd catalyst. A popular method is incorporating the carbon support with other metal compounds which can alter the metal-support interaction of the catalyst. A stronger metal-support interaction between the Pd nanoparticles and the support is confirmed to increase the electrocatalytic activity and stability of the FAOR. Various types of metal compounds were combined with the carbon as the Pd support, for instance, CeO_x [21], MoO_x [22], WO_3 [23], SiO_2 [24], $WMoO_x$ [25], MoO_3 [26], CuO [6], SnO_2 [27], and Sm_2O_3 [28]. Doping the carbon support with a heteroatom, such as N, P and B, was also reported to promote the FAOR catalytic activity. The mono- or dual-heteroatom doping of the carbon support for the Pd catalyst was also evaluated, such as Pd/N–C [29,30], Pd/N–C–TiO_2 [31], Pd/NP-C [32], Pd/NP-Coal-CNF [33] and Pd/BG [34]. In addition, a binary carbon supported Pd catalyst also performed well. For instance, the combined graphene and carbon black as the Pd support (Pd/GC) [35] and carbon black-embedded carbon nanofiber-supported Pd (Pd/CB-CNF) [36] improved the FAOR activity. In some studies, both of the above-mentioned strategies were combined in which the Pd alloy was supported on the modified carbon support. For example, PdMoP/BN-CNT [37], PdNi/N-G [38], PdSn/BN-G [39] and Pd_3Cu/CeO–C [40].

In addition to the afore-mentioned materials, transition metal dichalcogenides (TMDs) have gained interest for use in electrocatalyst applications due to their high abundance, low cost, and attractive electrochemical properties [41]. TMDs, such as MoS_2 and ReS_2, have been evaluated for DLFC anode electrocatalyst applications [42–45]. MoS_2 has emerged as a promising catalyst material for enhancing the electrocatalytic activity and stability for the oxidation of alcohols. A highly-active and stable catalyst was obtained by supporting Pt on the MoS_2/N–C for the methanol oxidation reaction [42]. A superior activity and stability for the oxidation of methanol, ethylene glycol and glycerol were also achieved on the MoS_2/NrGO supported Pt catalyst as compared to the commercial Pt/C catalyst [43]. A well-dispersed Pt on the MoS_2/rGO support was also obtained which displayed a higher electrocatalytic activity toward the methanol oxidation and formic acid oxidation than that of the Pt/C catalyst [44]. The addition of MoS_2 to the support of the Pt catalyst has already been shown to improve the CO-poisoning on the Pt catalyst and improve the electrocatalytic activity. These behaviors suggested that the addition of MoS_2 to the catalyst support is favorable for promoting the electrocatalytic activity regarding the oxidation of small organic molecules.

The objective of this study is to improve the electrocatalytic activity of the Pd-based catalyst for the formic acid oxidation. In a previous study conducted in our laboratory, the formic acid oxidation activity was improved by supporting Pd on a Vulcan XC-72-embedded carbon nanofiber (VECNF). The VECNF provided a higher surface area than if only the Vulcan XC-72 was used as the support. Moreover, embedding Vulcan XC-72, which is simultaneously heat treated with the electrospun polymer fiber, into the carbon nanofiber produces a stronger metal-support interaction. These features of the carbon support resulting in the enhancement of the FAOR activity [36]. Motivated by this finding, we proposed to add MoS_2 to the VECNF as the Pd support to further enhance the FAOR activity. To the best of the author's knowledge, the use of MoS_2 for the FAOR electrocatalyst is limited. In addition, Mo@Pd has been theoretically predicted as the most promising Pd alloy catalyst for the formic acid oxidation. It was determined that the direct pathway of the formic acid oxidation via the formate (HCOO) intermediate was most favored on the Mo@Pd alloy [5]. This provides a way to obtain an improved FAOR activity by adding a Mo-based material to the Pd catalyst. Therefore, MoS_2 nanoparticles and a Vulcan embedded carbon nanofiber (MoS-VECNF) was developed in this study as the Pd catalyst support. First, the MoS-VECNF support was prepared by electrospinning and heat treatment. Next, Pd nanoparticles were deposited by the polyol method with a 20 wt % Pd loading. The Pd/MoS-VECNF catalyst was characterized by XRD, SEM, EDX and XPS. Their FAOR activity and stability were then tested and compared to the MoS-only catalyst (Pd/VECNF). The weight ratio of MoS_2 to polyacrylonitrile (PAN) for the MoS-VECNF support was varied at 0.05, 0.10 and 0.15 to determine the optimum MoS_2 content.

The Pd/MoS-VECNF catalyst exhibited an excellent activity and stability for the FAOR as compared to the Pd/VECNF. This study provided a new approach to modify the catalyst support for improving the formic acid oxidation activity and stability of the Pd-based catalyst.

Experimental method

Carbon nanofiber support preparation

The electrospinning ink solution was prepared by dissolving Vulcan XC-72R (Fuel Cell Earth) and MoS_2 nanoparticles (US Research Nanomaterials, Inc.) in N,N-dimethylformamide (FUJIFILM Wako Pure Chemical Co., Ltd.) and sonicated for 30 min, then stirred for 1 h. Polyacrylonitrile (Sigma-Aldrich) was added to the solution and stirred for 5 h at 80 °C. The ink solution was then stirred overnight at room temperature. Afterwards, the solution was added to a 5-mL syringe and electrospun at the applied voltage of 25 kV, flow rate of 0.7 mL min^{-1}, spinneret-to-collector distance of 15 cm and 30% RH. The drum collector was covered with Al foil and rotated at the speed of 300 rpm. The electrospinning device was a NANON 03 electrospinning setup (MECC Co., Ltd., Japan). The electrospun nanofiber was stabilized under flowing N_2 and O_2 at 250 °C for 10 h. The stabilized nanofiber was then carbonized at 1000 °C for 1 h. Next, the carbonized nanofiber was steam-activated under humidified N_2 at 850 °C for 1 h. The molybdenum-containing nanofiber was prepared with different MoS_2 to PAN weight ratios (0.05, 0.10 and 0.15) which were designated as MoS-VECNF 0.05, MoS-VECNF 0.10 and MoS-VECNF 0.15, respectively. The nanofiber without MoS_2 (VECNF) was also prepared for comparison.

Catalyst preparation

Palladium (Pd) was deposited on the MoS_2/VECNF support by the polyol method. $PdCl_2$ (FUJIFILM Wako Pure Chemical Co., Ltd.) was dissolved in ethylene glycol (FUJIFILM Wako Pure Chemical Co., Ltd.) by sonication for 1 h, then stirred overnight at room temperature. MoS_2/VECNF was also dissolved in ethylene glycol by sonication and stirred for 3 h. The pH of the $PdCl_2$ in the ethylene glycol was adjusted to 11 by NaOH (in the ethylene glycol). Next, the $PdCl_2$ solution was stirred and heated at 160 °C for 3 h. The colloidal suspension was then added to the MoS_2/VECNF support solution. The pH of the mixture was adjusted to 1 by a 0.5 M HNO_3 solution and stirred overnight. The catalyst was filtered, washed with water, and finally dried overnight in a vacuum oven at 110 °C. A 20 wt% Pd loading was prepared in this study. The prepared catalyst was denoted as Pd/MoS-VECNF. A Pd/VECNF catalyst was also prepared by the same method for comparison.

Physical characterization

The MoS-VECNF support and the Pd/MoS-VECNF catalyst were physically characterized by using a scanning electron microscope-energy disperse X-ray (SEM-EDX, Hitachi High-Tech Corp., Japan) to determine the morphology of the carbon nanofiber. The X-ray diffraction (XRD) pattern from the X-ray diffractometer (Miniflex, Rigaku, Japan), using Cu Kα radiation operated at 2.7 kV and 30 mA, was used to determine the crystallite size of the Pd nanoparticles. The Pd face centered cubic (fcc) peak at 40° was considered for the calculation using Sherrer's formula:

$$d = \frac{0.9\,\lambda}{\beta \cos\theta} \tag{3}$$

where λ is the X-ray wavelength (1.54056 Å), β is the width of the peak at half height, and θ is the peak angle. The weight percentage of the Pd nanoparticles in the catalyst was determined by heating the prepared catalyst at 600 °C for 45 min in air. The residue weight was measured and the weight ratio of Pd in the residue was also determined by an EDX measurement. The X-ray photoelectron spectroscopy (XPS, JEOL Ltd., Japan) was conducted to determine the surface elemental composition and the chemical state of the catalyst element. The obtained data were analyzed using SpecSurf (ver. 1.9.3, JEOL) analysis software.

Electrochemical characterization

The electrochemical characterization of the catalysts was done using a conventional three-electrode electrochemical cell configuration and the data were recorded by a potentiostat/galvanostat (Automatic Polarization System HSV-110, Hokuto Denko Corp.). A glassy carbon electrode (GCE) with the diameter of 3 mm was the working electrode, a Pt wire was the counter electrode and a $Hg/HgSO_4$ electrode in a saturated K_2SO_4 solution was the reference electrode. All the potentials reported in this study are referred to the normal hydrogen electrode (NHE). The GCE was polished using an alumina slurry, then washed with distilled water. The catalyst ink was prepared by dispersing 5 mg of the catalyst in 320 μL of ethanol and 25 μL of a 5 wt% Nafion solution. After sonication for 1 h, 2.5 μL of the ink was pipetted on the cleaned GCE and naturally dried at room temperature for 30 min. For the electrocatalytic activity measurement, cyclic voltammetry (CV) was performed in a mixed solution of 0.5 M H_2SO_4 and 3 M HCOOH in the potential range of 0–1.20 V (vs. NHE) at the scan rate of 10 mV s^{-1}. The CV measurement was also conducted in the solution of 0.5 M H_2SO_4 containing 0.5 M HCOOH to compare the FAOR activity with other studies. To determine the stability of the synthesized catalyst, a chronoamperometry (CA) measurement for 3600s was conducted in the N_2-saturated 0.5 M H_2SO_4 with a 3 M HCOOH solution at the potential of 0.60 V (vs. NHE). To determine the CO-poisoning tolerance on the catalyst, the CO-stripping CV test was carried out. CO was bubbled into the electrolyte while the electrode potential was maintained at 0.2 V (vs. NHE) for 45 min to adsorb CO onto the catalyst layer. The dissolved CO was then purged out by bubbling N_2 for 15 min. Next, the CO-stripping voltammogram was recorded in the potential range of 0–1.20 V (vs. NHE). The obtained current was normalized with the Pd loading deposited on the GCE to obtain the mass activity (mA mg_{Pd}^{-1}). Prior to each measurement, the solution was purged with N_2 for 30 min to remove the O_2 in the solution. All the measurements were conducted at room temperature.

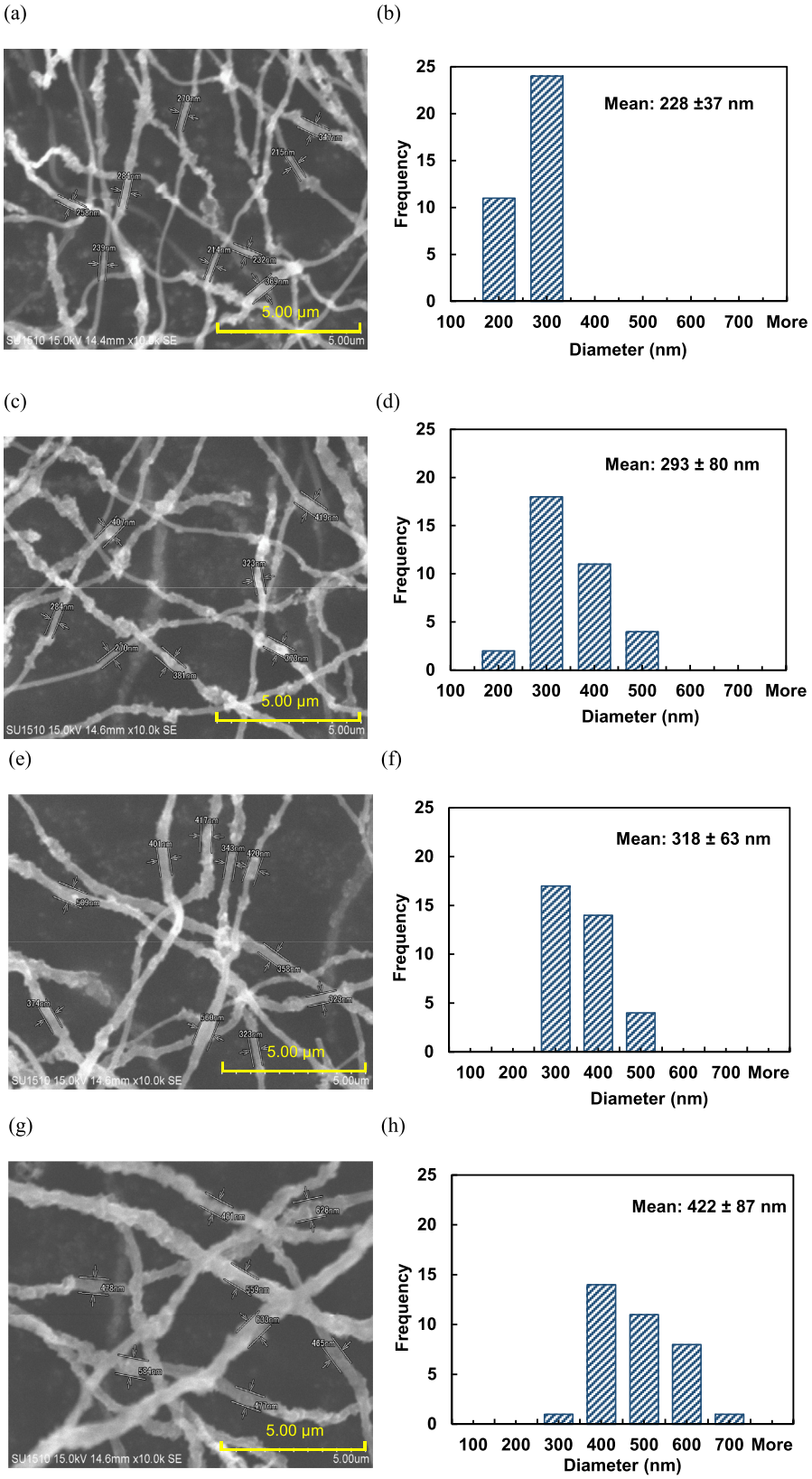

Fig. 1 – SEM images and the corresponding fiber diameter distribution histograms of heat-treated VECNF (a,b), MoS-VECNF 0.05 (c,d), MoS-VECNF 0.10 (e,f), and MoS-VECNF 0.15 (g,h).

Results and discussion

Physical characterization

The carbon supports prepared prior to the Pd deposition were characterized by SEM and EDX to determine their morphology features. Fig. 1 shows SEM images of the heat-treated VECNF and MoS-VECNF with different MoS contents and their corresponding distribution of the fiber diameter histograms. The average fiber diameters after heat treatment of the VECNF, MoS-VECNF 0.05, MoS-VECNF 0.10 and MoS-VECNF 0.15 were 228 ± 37, 293 ± 80, 318 ± 63 and 422 ± 87 nm, respectively. The MoS-VECNF supports show a rougher structure and bigger fiber diameter as compared to the VECNF support. The average fiber diameter of the MoS-VECNF increased as the MoS_2 nanoparticle content increased. MoS-VECNF 0.15 showed larger beads on the nanofiber structure than the 0.05 and 0.10 ones. The elemental mapping of the MoS-VECNF 0.10 support shown in Fig. 2 revealed that the C, Mo, and S were uniformly distributed on the nanofiber. The XRD patterns in Fig. S1 show the strong peaks of MoS_2 in the carbon support as the MoS_2 content increased. Thus, it was confirmed that the MoS_2 was embedded in the nanofiber structure.

The Pd loading of all the prepared catalysts was 19–21 wt %. The XRD patterns for the Pd/VECNF and Pd/MoS-VECNF with the different prepared MoS_2 catalyst contents are shown in Fig. 3. A broad diffraction peak observed at ca. 25° for all the catalyst samples represents the (002) carbon plane. Strong diffraction peaks at about 40.1, 46.5, and 68.3° were attributed to the (111), (200) and (220) plane, respectively

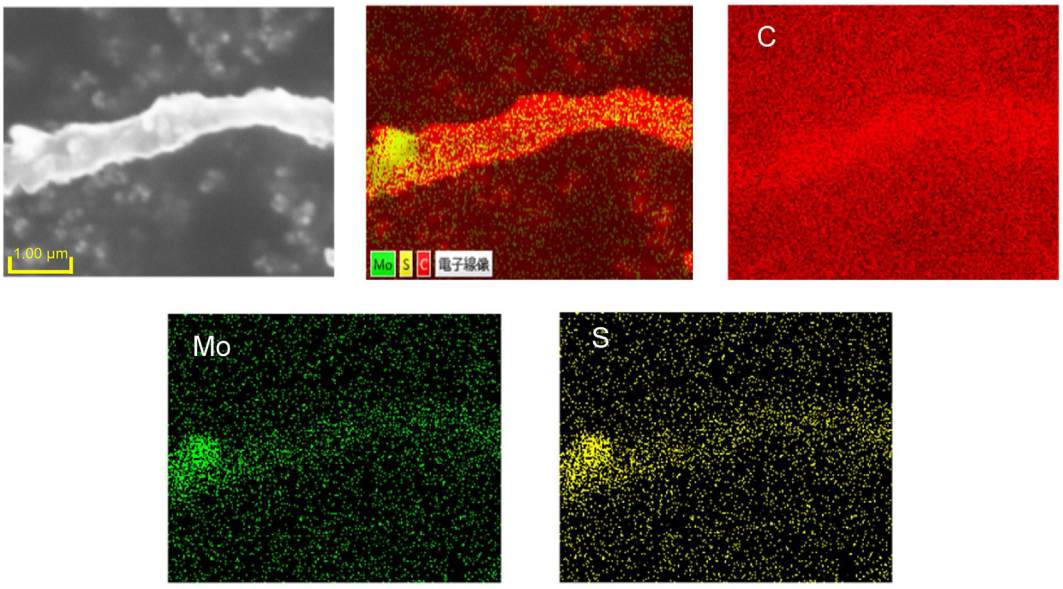

Fig. 2 – EDX elemental mapping image of the Pd/MoS-VECNF 0.10 catalyst.

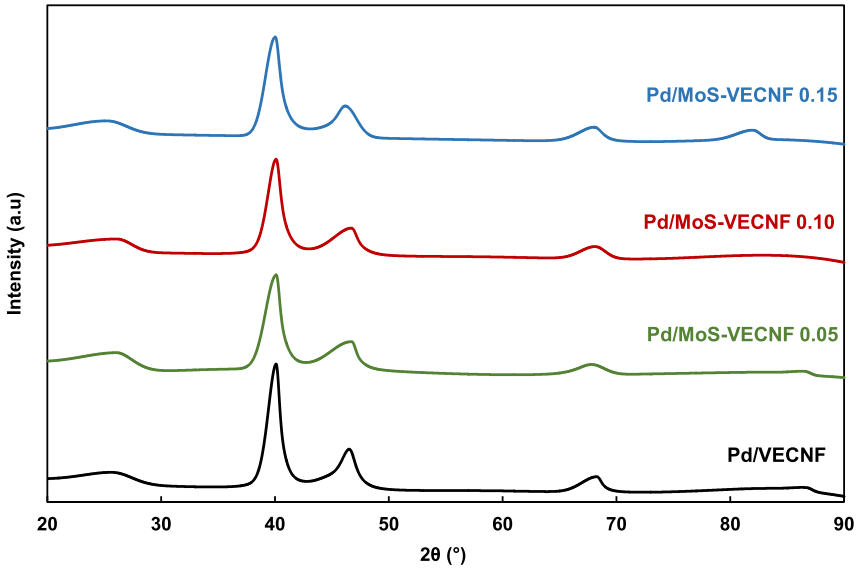

Fig. 3 – XRD patterns of Pd/VECNF and Pd/MoS-VECNF catalysts (0.05, 0.10 and 0.15 g of MoS_2 content).

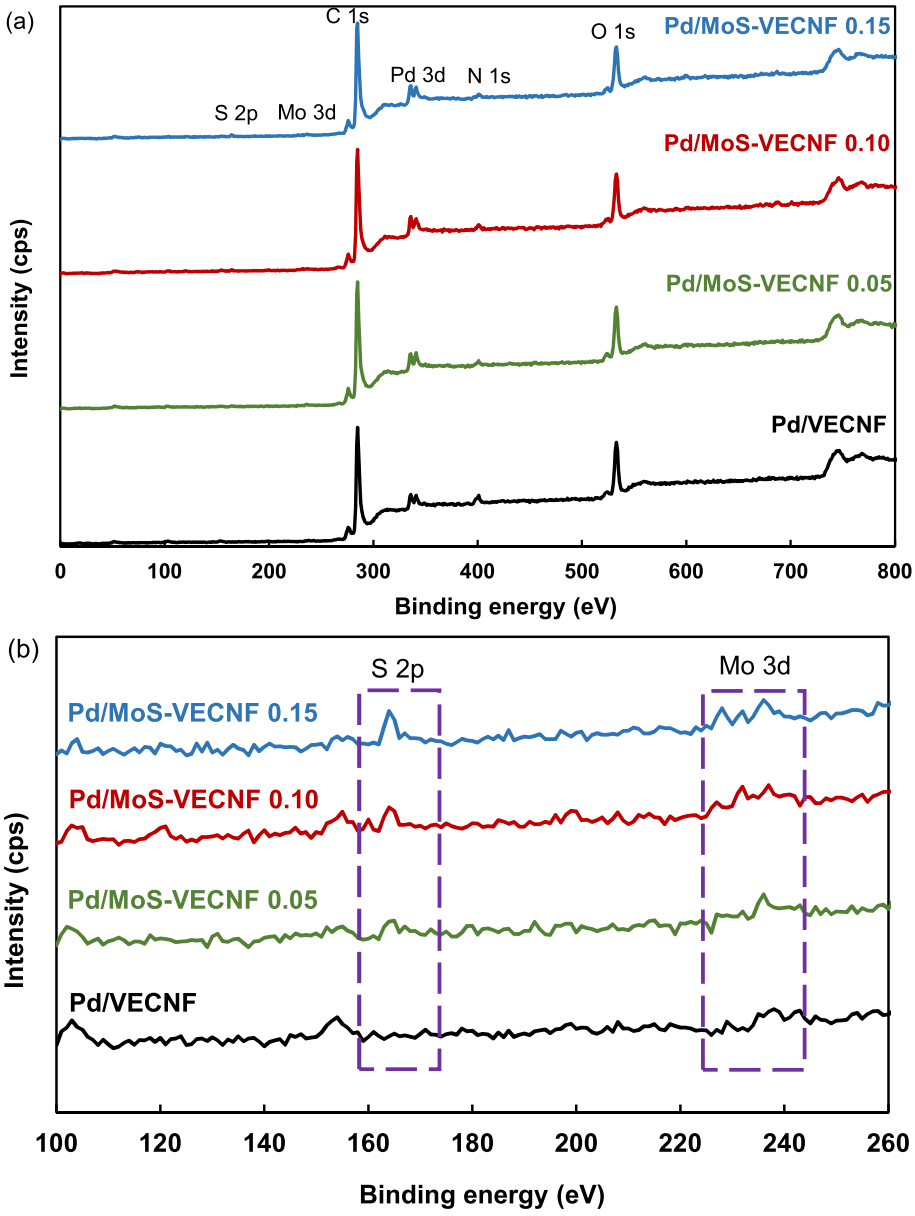

Fig. 4 – XPS spectra for all the element peaks (a) and Mo 3d and S 2p peak region (b) for all the catalyst samples.

which is the face-centered cubic (fcc) structure of Pd also present in all the catalyst samples. The crystallite size of the Pd based on the (111) peak was 6.9, 5.5, 6.1 and 5.6 nm for Pd/VECNF, Pd/MoS-VECNF 0.05, Pd/MoS-VECNF 0.10, and Pd/MoS-VECNF 0.15, respectively. The addition of MoS_2 to the catalyst support resulted in a slightly smaller Pd crystallite size as compared to the pure VECNF supported Pd catalyst. Therefore, it can be inferred that the presence of MoS_2 in the catalyst support is not influencing the Pd crystal structure but affecting the Pd crystallite size which was also reported in other studies [25]. The MoS_2 peaks are invisible after the Pd deposition due to the low MoS_2 loading which causes the coverage of MoS_2 by the Pd [46,47]. Thus, the existence of the MoS_2 was confirmed by XPS characterization as further discussed in the next section.

The surface composition and the chemical state of each element were analyzed based on the XPS spectra for each studied catalyst. Each element curve was fitted by using a Shirley-type background and the Gauss-Lorentz equation. Fig. 4 (a) shows the wide scan spectra for all the catalyst samples. The C1s, O1s, N1s, and Pd 3d peaks were observed in the spectra for all the catalyst samples. As the content of MoS_2 is relatively low, the Mo and S peaks are indistinct in the figure as compared to the other element peaks. Fig. 4 (b) shows the spectra focusing on the binding energy for the Mo and S elements. Peaks corresponding to the Mo 3d and S 2p were distinctly observed in all the Pd/MoS-VECNF catalyst samples. As the MoS_2 content increased, sharp peaks appeared and assigned to the Mo 3d and S 2p species. Therefore, it was confirmed that the MoS_2 is present in the Pd/MoS-VECNF catalyst. The atomic composition obtained from the quantification of the XPS spectra is shown in Table 1. There was a slight difference in the Mo content between the Pd/MoS-VECNF 0.10 and Pd/MoS-VECNF 0.15 catalysts which was 0.47 and 0.50,

Table 1 – Elemental composition based on the XPS analysis.

Catalyst	Element content (at.%)					
	C	N	O	Pd	Mo	S
Pd/VECNF	79.39	4.37	13.69	2.55	–	–
Pd/MoS-VECNF 0.05	81.03	3.71	12.17	2.53	0.20	0.36
Pd/MoS-VECNF 0.10	80.20	3.06	12.95	2.60	0.47	0.72
Pd/MoS-VECNF 0.15	80.96	2.93	11.97	2.61	0.50	1.04

respectively, due to an error by a small peak among the fittings. However, S of which its peak clearly showed compared to that of the Mo content proportionally increased with the added MoS_2. Therefore, it is considered that the Mo content also increased with the increasing MoS_2 content.

To determine the chemical state and possible interaction between the metal and support, the Pd 3d spectra were analyzed. The curve fitted Pd 3d peaks for all the catalyst samples shown in Fig. 5 clearly indicated the existence of two

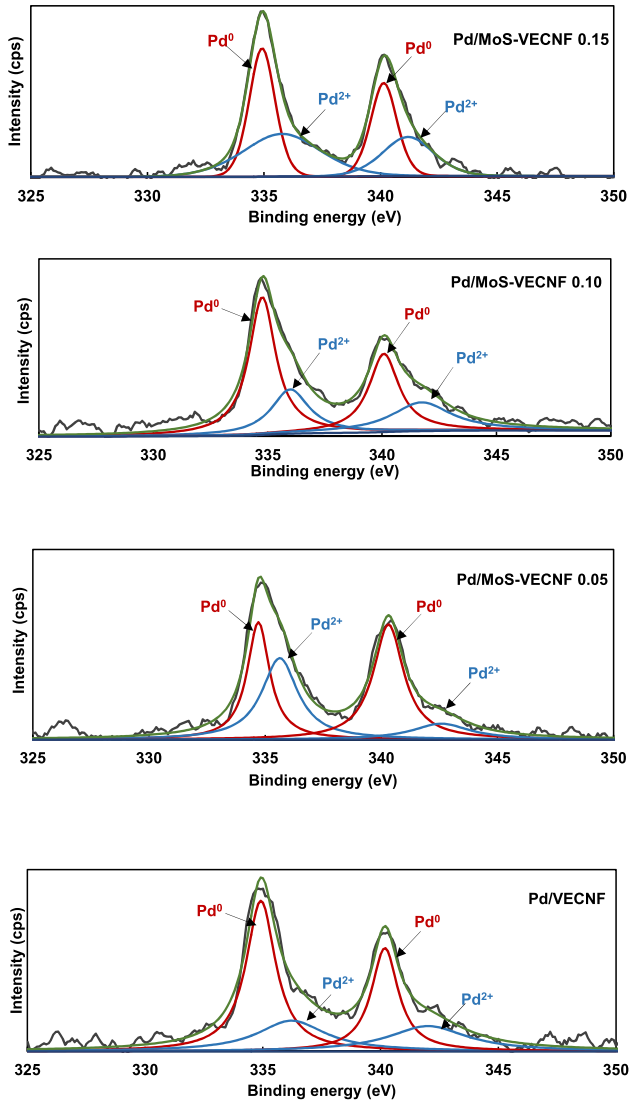

Fig. 5 – XPS spectra of Pd 3d for the Pd/VECNF and Pd/MoS-VECNF (0.05, 0.10, 0.15) catalysts.

Table 2 – Binding energies of Pd3d for the Pd/VECNF and Pd/MoS-VECNF catalysts.

Catalyst	Pd $3d_{5/2}$ binding energy (eV)	Chemical state	Relative intensity (%)
Pd/VECNF	334.92	Pd^0	67
	336.22	Pd^{2+}	33
Pd/MoS-VECNF 0.05	334.70	Pd^0	62
	335.63	Pd^{2+}	38
Pd/MoS-VECNF 0.10	334.77	Pd^0	65
	335.99	Pd^{2+}	35
Pd/MoS-VECNF 0.15	334.92	Pd^0	52
	335.77	Pd^{2+}	48

chemical states of the Pd atom in each catalyst. The Pd $3d_{5/2}$ and Pd $3d_{3/2}$ regions were deconvoluted into two doublet peaks corresponding to the metallic state (Pd^0) and +2 oxidation state (Pd^{2+}). The binding energy (BE) for Pd^0 and Pd^{2+} of each catalyst is summarized in Table 2. The BE for Pd^0 and Pd^{2+} in the Pd/MoS-VECNF catalyst was shifted to a lower value as compared to the Pd/VECNF catalyst. The BE of Pd^0 is lower by 0.22 eV and 0.15 eV for Pd/MoS-VECNF 0.05 and Pd/MoS-VECNF 0.10, respectively. Meanwhile, the BE of Pd^0 for the Pd/MoS-VECNF 0.15 catalyst was not shifted. However, the shifts in the Pd^{2+} BE are greater in all the Pd/MoS-VECNF catalysts. The shifting of the binding energy represents the strong interaction between the Pd nanoparticles and MoS-VECNF support. Furthermore, the negative shift of the Pd 3d BE is beneficial to weaken the bond between the Pd and intermediates species, such as CO, and thus, improving the CO anti-poisoning ability of the Pd catalyst [48]. Therefore, the shifting of the Pd 3d BE in the Pd/MoS-VECNF catalyst suggested that the electronic nature of Pd is altered by the addition of MoS_2 that can contribute to promoting the FAOR activity [49]. A similar occurrence was also found in the study reported by Tang et al. in which the BE of the Pt supported on the MoS–N-doped C is shifted to a lower value than that of the Pt/C catalyst [42]. In addition, it was found that the Pd^{2+} species is higher in Pd/MoS-VECNF than in the Pd/VECNF catalyst, but the Pd^0 species still dominates in all the catalyst samples which is beneficial for the formic acid oxidation. The presence of Pd^{2+} can be considered as an insignificant factor for the electrocatalytic activity because it could be reduced to Pd^0 again by the formic acid oxidation [6]. Thus, based on these characteristics, an improved FAOR activity is expected for the catalyst with the presence of MoS_2.

Electrochemical characterization

The electrochemical characteristics of the Pd/VECNF and Pd/MoS-VECNF catalysts were determined by cyclic voltammetry (CV) measurements. Based on the CV measurement, the electrochemical surface area (ECSA) and the electrocatalytic activity for the FAOR of the catalysts were established. The CV was conducted in a N_2-bubbled 0.5 M H_2SO_4 solution in the potential range from 0 to 1.20 V (vs. NHE) to determine the ECSA as shown in Fig. 6 (a). The CV curve shows a distinct peak of hydrogen desorption and adsorption in the potential region of 0.04–0.25 V (vs. NHE) for all the catalyst samples. The ECSA value was estimated based on the

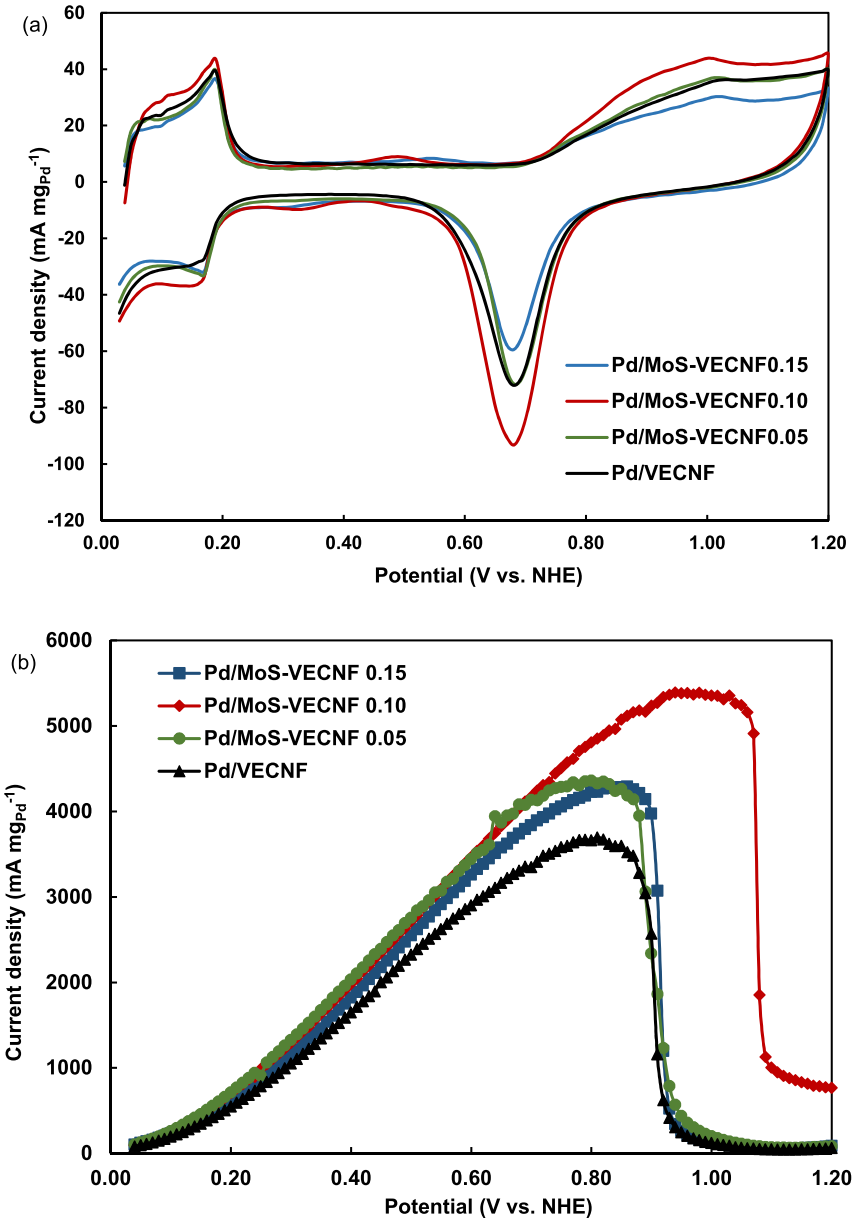

Fig. 6 – Cyclic voltammetry curves in N_2-saturated 0.5 M H_2SO_4 solution (a) and forward scan of FAOR curve in 0.5 M H_2SO_4 + 3 M HCOOH (b) for Pd/VECNF and Pd/MoS-VECNF (scan rate is 10 mV s^{-1}).

hydrogen desorption region which can be calculated by the following equation [50]:

$$ECSA = \frac{Q_H}{210 \times M} \times 100 \quad (4)$$

Q_H (C) is the charge exchange during the hydrogen electrolysis, 210 (μC cm^{-2}) is the charge required to oxidize the hydrogen in a monolayer, and M (g) is the Pd loading on the working electrode. The ECSA for the Pd/VECNF, Pd/MoS-VECNF 0.05, Pd/MoS-VECNF 0.10, and Pd/MoS-VECNF 0.15 catalysts was 170, 174, 176 and 160 m^2 g^{-1}, respectively. Based on these values, it can be deduced that the ECSA slightly increases with the addition of MoS_2 in the Pd support as compared to the pure VECNF-supported Pd. A higher ECSA for the catalyst infers that more electrocatalytic active sites are provided by the catalyst which promotes the electrocatalytic activity [51]. However, as the MoS_2 content increased to 0.15, the ECSA slightly decreased which is due to coverage of the Pd by the excess amount of MoS_2 that reduces the exposure of the active site. Based on these ECSA values, it can be predicted that the FAOR activity will be higher for Pd/MoS-VECNF as compared to the catalyst without MoS_2.

The CV measurement was conducted in a 0.5 M H_2SO_4 solution containing 3 M formic acid to determine their electrocatalytic behavior towards the FAOR activity. Fig. 6 (b) shows the forward scan of the CV curve for the Pd/VECNF and the prepared Pd/MoS-VECNF catalysts. The CV curve indicates the current density normalized by the mass of the Pd. The FAOR activity of the catalyst was determined based on the peak current density value. It was noted that the Pd/MoS-VECNF catalyst shows a higher FAOR activity than that of the Pd/VECNF catalyst for all the MoS_2 contents. The achieved peak

current density was 3697, 4363, 5395 and 4295 mA mg_{Pd}^{-1} for Pd/VECNF, Pd/MoS-VECNF 0.05, Pd/MoS-VECNF 0.10 and Pd/MoS-VECNF 0.15, respectively. The peak current density achieved its optimum value with the Pd/MoS-VECNF 0.10 catalyst which was 1.46 times greater with respect to the Pd/VECNF catalyst. The increase in the peak current density is in good agreement with the prediction based on the shifting of the Pd 3d binding energy that implies a strong metal-support interaction produces a better FAOR activity. The Pd/MoS-VECNF 0.10 catalyst displayed the highest peak current density as compared to the 0.05 and 0.15 catalysts due its highest Pd^0 content. It is suggested that the higher the Pd^0 content, the better the catalytic activity [52]. The peak current density decreased as the MoS_2 content increased to 0.15 which can be explained from the BE of the Pd^0 that is not shifted, inferring a weaker metal-support interaction as compared to Pd/MoS-VECNF 0.05 and Pd/MoS-VECNF 0.10. This indicated that the electronic modification is insignificant in the Pd/MoS-VECNF 0.15 catalyst, hence reducing the FAOR activity. This electronic modification is important to inhibit the intermediate adsorption on Pd and stimulate the desorption of H_2 from the catalyst [6].

However, the FAOR activity of the Pd/MoS-VECNF 0.15 catalyst is better than that of Pd/VECNF. The reason for this can be ascribed to the hydrogen spillover effect with the presence of MoS_2 in the catalyst. The hydrogen spillover is when the hydrogen from the dehydrogenation that adsorbed on the Pd is transferred onto the MoS_2 surface. Consequently, more Pd active sites are available for further adsorption and oxidation of the formic acid [53]. This is because MoS_2 is an efficient catalyst for the hydrogen evolution reaction (HER) thus hydrogen can be easily adsorbed on the MoS_2 [54]. In the study done by J. Chang et al. an effective HER catalyst (Ni_2P) was added to the Pd carbon support for the formic acid oxidation. The strong metal-support interaction and hydrogen spillover effect provided by the Ni_2P to the catalyst contributed to the electrocatalytic activity improvement [55]. In some studies reported [56,57], sulfur-containing materials are not preferable as a Pd-based catalyst support since they may generate SO_x, which poisons the Pd catalyst. However, the MoS_2 content in the catalysts synthesized in this study is relatively low. Therefore, the poison effect of SO_x on the Pd catalyst might not be severe. The poison effect of SO_x on the Pd-based catalyst should be considered in future studies.

Besides the catalytic activity, the catalyst stability is an important factor to meet the commercialization requirements. The FAOR stability of the Pd/MoS-VECNF and Pd/VECNF catalyst samples was tested by chronoamperometry (CA) in a 0.5 M H_2SO_4 solution containing 3 M HCOOH at 0.6 V (vs. NHE) for 3600 s. The Pd/MoS-VECNF catalyst maintained a higher current density than the Pd/VECNF catalyst over the entire test period as shown in Fig. 7 (a). Based on the percentage of the relative current in Fig. 7 (b), the Pd/MoS-VECNF catalyst demonstrated a better electrocatalytic stability than the Pd/VECNF catalyst. The Pd/MoS-VECNF 0.10 catalyst showed the highest residual current density after the 3600 s CA test, followed by the Pd/MoS-VECNF 0.05, Pd/MoS-VECNF 0.15 and Pd/VECNF catalysts. The current density retained after the 3600 s testing for Pd/MoS-VECNF 0.10 is 6 times higher than that of the Pd/VECNF catalyst. The curve pattern for the first 1500 s shows a slow reduction in the current

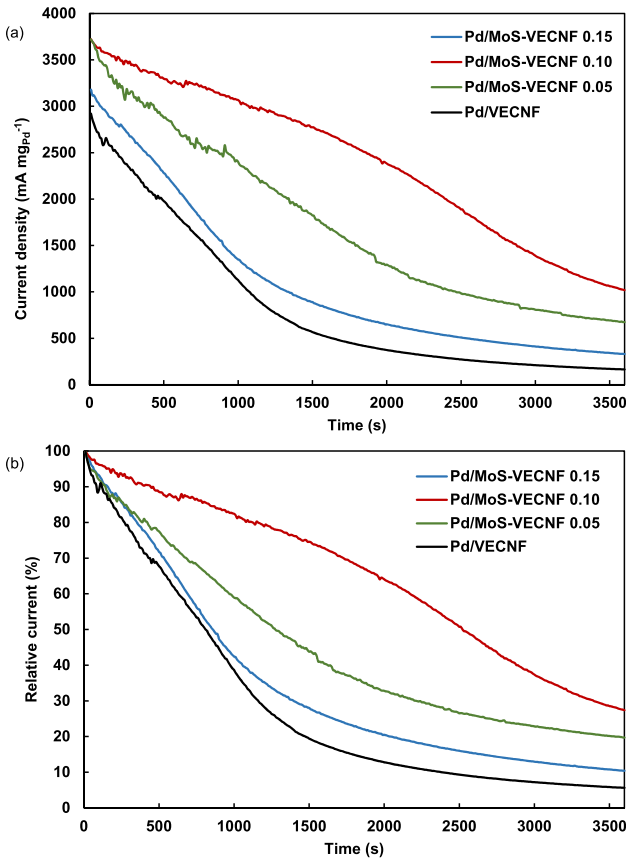

Fig. 7 – Chronoamperometric curves (a) and relative current (b) of Pd/VECNF and Pd/MoS-VECNF catalyst in 0.5 M H_2SO_4 + 3 M HCOOH solution at 0.60 V (vs. NHE) for 3600 s.

density for the Pd/MoS-VECNF 0.10 whereas a dramatic decrease in the current density for Pd/VECNF was observed. A superior stability can be achieved by the addition of MoS_2 to the catalyst with the appropriate content. The CO anti-poisoning ability of the catalyst is enhanced with the presence of MoS_2 in the catalyst [42].

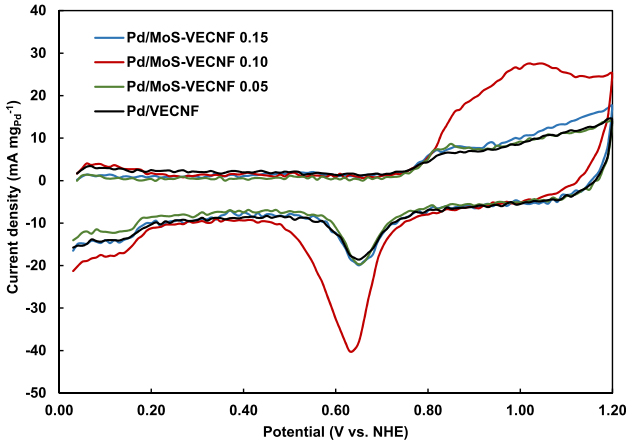

Fig. 8 – CO-stripping voltammetry curve for Pd/VECNF and Pd/MoS-VECNF (0.05, 0.10 and 0.15) catalyst in 0.5 M H_2SO_4 at the scan rate of 10 mVs^{-1}.

Table 3 – Comparison to recent studies of Pd-based catalyst for FAOR.

Catalyst	Pd loading (wt.%)	Electrolyte solution	Peak current density (mA mg_{Pd}^{-1})	References
Pd/$(C_{16}mim)_3PMo_{12}O_{40}$/NP-CFs	20	0.5 M H_2SO_4 + 0.5 M HCOOH	754	[61]
Pd/xCuO-CNT	10	0.5 M H_2SO_4 + 0.5 M HCOOH	1904	[6]
Pd/WMOx-C	15	0.5 M H_2SO_4 + 0.5 M HCOOH	912	[25]
Pd/adenine modified-G	14.5	0.5 M H_2SO_4 + 0.5 M HCOOH	1350	[62]
Pd/SnO_2–C	12.5	0.5 M H_2SO_4 + 0.5 M HCOOH	1001	[27]
Pd/MoO_3–C	10	0.5 M H_2SO_4 + 0.5 M HCOOH	~1000	[26]
Pd/MoS-VECNF	20	0.5 M H_2SO_4 + 0.5 M HCOOH	1925	This study

To determine the CO anti-poisoning ability of the prepared catalyst, a CO stripping test was conducted as shown in Fig. S2. The second cycle after the CO stripping showed hydrogen adsorption/desorption peaks suggesting that the oxidation of CO was complete [58]. Fig. 8 shows the CO stripping curve for all the catalysts. It was found that the onset potential in which the starting potentials for the CO oxidation of the Pd/VECNF and Pd/MoS-VECNF catalysts showed similar values. A similar onset potential value was also observed when the Pd support was modified in the study done by Y. Bao et al. [38]. Their findings showed a more significant improvement of the CO anti-poisoning ability by alloying the Pd with Ni than supporting the Pd with different type of carbon. Similar to their study, the CO oxidation peak area of the Pd/MoS-VECNF 0.10 catalyst is broader than that of the other catalysts. This indicated that the CO can be more easily removed from the Pd/MoS-VECNF 0.10 [52,59]. Hence, the Pd/MoS-VECNF 0.10 catalyst showed the highest FAOR activity and stability. It can be deduced that the appropriate content of MoS_2 in the catalyst support is needed.

For this study, the FAOR activity measurement was evaluated using the 3 M HCOOH solution which is more concentrated than most reported in other studies to mimic the practical conditions of the DFAFC operation which typically used 3 M or higher HCOOH solutions [60]. For comparison purposes, we also measured the FAOR activity of the optimized Pd/MoS-VECNF catalyst in 0.5 M H_2SO_4 containing the 0.5 M HCOOH solution. The FAOR activity of our catalyst and the most recent Pd-based catalyst reported for the DFAFC anode application is summarized in Table 3. The listed catalysts are using the support modification strategy to enhance the FAOR activity. The Pd/MoS-VECNF catalyst prepared in our study is the highest when compared to the other studies. Therefore, the catalyst introduced in this study has a significant potential for DFAFC applications.

Conclusions

The MoS-VECNF supported Pd catalyst was successfully synthesized to improve the electrocatalytic activity and stability towards formic acid oxidation for DFAFC anode applications. Based on the electrochemical measurement, the activity and stability for the FAOR is improved by the addition of MoS_2 in the carbon nanofiber support when compared to no MoS_2. The optimum amount of MoS_2 is 0.10 g with the peak current density of 5395 mA mg_{Pd}^{-1}. The achieved peak current density is 1.46 times higher than that of the Pd/VECNF catalyst. The superior stability was also shown by the Pd/MoS-VECNF catalyst when compared to the Pd/VECNF catalyst. A stronger metal-support interaction provided by the presence of MoS_2 in the carbon support contributes to the further improvement of the FAOR activity and stability. Therefore, the MoS-VECNF introduced here is promising as the Pd support to achieve a high performance for DFAFC applications.

Declaration of competing interest

The authors declare that they have no known competing financial interests or personal relationships that could have appeared to influence the work reported in this paper.

Acknowledgement

This study was supported by JSPS KAKENHI 22H01858, 21H02037 and New Energy and Industrial Technology Development Organization (NEDO) JPNP20004.

Appendix A. Supplementary data

Supplementary data to this article can be found online at https://doi.org/10.1016/j.ijhydene.2023.06.004.

REFERENCES

[1] Dutta I, Chatterjee S, Cheng H, Parsapur RK, Liu Z, Li Z, et al. Formic acid to power towards low-carbon economy. Adv Energy Mater 2022;12(15):1–17.
[2] Chen X, Granda-Marulanda LP, McCrum IT, Koper MTM. How palladium inhibits CO poisoning during electrocatalytic formic acid oxidation and carbon dioxide reduction. Nat Commun 2022;13(1):1–11.
[3] Wang H, Chen H, Wang HQ, Ou CR, Li R, Liu HB. Synthesis of ultrafine low loading Pd–Cu alloy catalysts supported on graphene with excellent electrocatalytic performance for formic acid oxidation. Int J Hydrogen Energy 2020;45(18):10735–44.
[4] Feng L, Chang J, Jiang K, Xue H, Liu C, Cai W. Nanostructured palladium catalyst poisoning depressed by cobalt phosphide in the electro-oxidation of formic acid for fuel cells. Nano Energy 2016:355–61.
[5] Sui L, An W, Feng Y, Wang Z, Zhou J, Hur SH. Bimetallic Pd-Based surface alloys promote electrochemical oxidation of formic acid: mechanism, kinetics and descriptor. J Power Sources 2020;451:227830.

[6] Maturost S, Themsirimongkon S, Saipanya S, Fang L, Pongpichayakul N, Jakmunee J, et al. Carbon nanotube-copper oxide-supported palladium anode catalysts for electrocatalytic enhancement in formic acid oxidation. Int J Hydrogen Energy 2022;47(8):5585–98.
[7] Wang X, Xia Y. Electrocatalytic performance of PdCo-C catalyst for formic acid oxidation. Electrochem Commun 2008;10:1644–6.
[8] Shen T, Lu Y, Gong M, Zhao T, Hu Y, Wang D. Optimizing formic acid electro-oxidation performance by restricting the continuous Pd sites in Pd-Sn nanocatalysts. ACS Sustainable Chem Eng 2020;8(32):12239–47.
[9] Wu D, Zheng Z, Gao S, Cao M, Cao R. Mixed-phase PdRu bimetallic structures with high activity and stability for formic acid electrooxidation. Phys Chem Chem Phys 2012;14(22):8051–7.
[10] Wang X, Tang Y, Gao Y, Lu T. Carbon-supported Pd-Ir catalyst as anodic catalyst in direct formic acid fuel cell. J Power Sources 2008;175(2):784–8.
[11] Goswami C, Saikia H, Tada K, Tanaka S, Sudarsanam P, Bhargava SK, et al. Bimetallic palladium-nickel nanoparticles anchored on carbon as high-performance electrocatalysts for oxygen reduction and formic acid oxidation reactions. ACS Appl Energy Mater 2020;3(9):9285–95.
[12] Goswami C, Saikia H, Jyoti Borah B, Jyoti Kalita M, Tada K, Tanaka S, et al. Boosting the electrocatalytic activity of Pd/C by Cu alloying: insight on Pd/Cu composition and reaction pathway. J Colloid Interface Sci 2021;587:446–56.
[13] Shen T, Chen S, Zeng R, Gong M, Zhao T, Lu Y, et al. Tailoring the antipoisoning performance of Pd for formic acid electrooxidation via an ordered PdBi intermetallic. ACS Catal 2020;10(17):9977–85.
[14] Caglar A, Ulas B, Cogenli MS, Yurtcan AB, Kivrak H. Synthesis and characterization of Co, Zn, Mn, V modified Pd formic acid fuel cell anode catalysts. J Electroanal Chem 2019;850:113402.
[15] Kankla P, Butburee T, Chanlek N, Sattayaporn S, Luksirikul P. Enhanced performance of bimetallic Pd-based electrocatalysts for formic acid oxidation. Top Catal 2023:0123456789.
[16] Jung WS, Han J. Enhanced stability of PdPtAu alloy catalyst for formic acid oxidation. Kor J Chem Eng 2021;38(11):2229–34.
[17] Chen Y, Niu HJ, Feng YG, Wu JH, Wang AJ, Huang H, et al. Three-dimensional hierarchical urchin-like PdCuPt nanoassembles with zigzag branches: a highly efficient and durable electrocatalyst for formic acid oxidation reaction. Appl Surf Sci 2020;510:145480.
[18] Ma Y, Li Y, Li P, Li Q. Facile one-pot synthesis of carbon supported PdCuCo nanoalloy catalysts for formic acid electrooxidation. Int J Electrochem Sci 2019;14(1):743–54.
[19] Er OF, Caglar A, Ulas B, Kivrak H, Kivrak A. Novel carbon nanotube supported Co@Ag@Pd formic acid electrooxidation catalysts prepared via sodium borohydride sequential reduction method. Mater Chem Phys 2020;241(August 2019):122422.
[20] Kivrak H, Aktas N. Promoting formic acid and ethylene glycol electrooxidation activity on Ga modified Pd based catalysts. Int J Hydrogen Energy 2022;47(83):35265–74.
[21] Feng L, Yang J, Hu Y, Zhu J, Liu C, Xing W. Electrocatalytic properties of PdCeO x/C anodic catalyst for formic acid electrooxidation. Int J Hydrogen Energy 2012;37(6):4812–8.
[22] Feng L, Cui Z, Yan L, Xing W, Liu C. The enhancement effect of MoOx on Pd/C catalyst for the electrooxidation of formic acid. Electrochim Acta 2011;56(5):2051–6.
[23] Feng L, Yan L, Cui Z, Liu C, Xing W. High activity of Pd-WO3/C catalyst as anodic catalyst for direct formic acid fuel cell. J Power Sources 2011;196(5):2469–74.
[24] Shan J, Zeng T, Wu W, Tan Y, Cheng N, Mu S. Enhancement of the performance of Pd nanoclusters confined within ultrathin silica layers for formic acid oxidation. Nanoscale 2020;12(24):12891–7.
[25] Li J, Fu Y, Xie J, Jia X, Kang Y, Zhang L. Rational design of defect-rich tungsten-molybdenum oxide modified carbon supported Pd as superior performances electrocatalyst for formic acid oxidation. Int J Hydrogen Energy 2022;47(35):15742–52.
[26] Jin J, Hu S, Zhang X, Sun S. Effect of MoO3 on Pd nanoparticles for efficient formic acid electrooxidation. Int J Hydrogen Energy 2023;48(41):15483–91.
[27] Wang J, Feng M, Hu S, Zhang X. The effect of SnO2 on enhancing electrocatalytic property of palladium toward formic acid oxidation. Int J Hydrogen Energy 2023;48(41):15492–503.
[28] Sofian M, Nasim F, Ali H, Nadeem MA. Sm2O3 promoted Pd/rGO electrocatalyst for formic acid oxidation. Int J Hydrogen Energy 2023;48(43):16370–80.
[29] Sun N, Wang M, Chang J, Ge J, Xing W, Shao G. Nitrogen-doped carbon black supported Pd nanoparticles as an effective catalyst for formic acid electro-oxidation reaction. Front Energy 2017;11(3):310–7.
[30] Chang J, Sun X, Feng L, Xing W, Qin X, Shao G. Effect of nitrogen-doped acetylene carbon black supported Pd nanocatalyst on formic acid electrooxidation. J Power Sources 2013;239:94–102.
[31] Qin YH, Li Y, Lam T, Xing Y. Nitrogen-doped carbon-TiO2 composite as support of Pd electrocatalyst for formic acid oxidation. J Power Sources 2015;284:186–93.
[32] Lu C. Nitrogen and phosphorus self-doped carbon supported palladium as highly efficient electrocatalysts for formic acid oxidation. Int J Electrochem Sci 2021;16:210555.
[33] Lou M, Wang R, Zhang J, Tang X, Wang L, Guo Y, et al. Optimized synthesis of nitrogen and phosphorus dual-doped coal-based carbon fiber supported Pd catalyst with enhanced activities for formic acid electrooxidation. ACS Appl Mater Interfaces 2019;11(6):6431–41.
[34] Xie Y, Wang J, Huang X, Luo B, Yu W, Shao L. Palladium nanoparticles supported on graphene sheets incorporating boron oxides (BxOy) for enhanced formic acid oxidation. Electrochem Commun 2017;74:48–52.
[35] Lv M, Li W, Liu H, Wen W, Dong G, Liu J, et al. Enhancement of the formic acid electrooxidation activity of palladium using graphene/carbon black binary carbon supports. Cuihua Xuebao/Chinese J Catal 2017;38(5):939–47.
[36] Mohamed Aslam N, Tsujiguchi T, Osaka Y, Kodama A. The origins of the high performance of Pd catalysts supported on carbon black-embedded carbon nanofiber for formic acid oxidation. Appl Sci 2019;9(24):5542.
[37] Liu F, Zhu Z, Fan J, Li Q, Min Y, Xu Q. Ternary PdMoP nanoparticles anchored on boron-nitrogen functionalized CNTs for high-efficiency formic acid electrooxidation. ACS Sustainable Chem Eng 2020;8(47):17587–96.
[38] Bao Y, Zha M, Sun P, Hu G, Feng L. PdNi/N-doped graphene aerogel with over wide potential activity for formic acid electrooxidation. J Energy Chem 2021;59:748–54.
[39] Chen D, Pei S, He Z, Shao H, Wang J, Wang K, et al. High active pdsn binary alloyed catalysts supported on B and N codoped graphene for formic acid electro-oxidation. Catalysts 2020;10(7).
[40] Goswami C, Borah BJ, Das R, Tada K, Tanaka S, Prosvirin IP, et al. CeO2 promotes electrocatalytic formic acid oxidation of Pd-based alloys. J Alloys Compd 2023;948:169665.
[41] Ahmaruzzaman M, Gadore V. MoS2 based nanocomposites: an excellent material for energy and environmental applications. J Environ Chem Eng 2021;9(5):105836.

[42] Tang B, Lin Y, Xing Z, Duan Y, Pan S, Dai Y, et al. Porous coral reefs-like MoS2/nitrogen-doped bio-carbon as an excellent Pt support/co-catalyst with promising catalytic activity and CO-tolerance for methanol oxidation reaction. Electrochim Acta 2017;246:517–27.
[43] Ramakrishnan S, Karuppannan M, Vinothkannan M, Ramachandran K, Kwon OJ, Yoo DJ. Ultrafine Pt nanoparticles stabilized by MoS 2/N-doped reduced graphene oxide as a durable electrocatalyst for alcohol oxidation and oxygen reduction reactions. ACS Appl Mater Interfaces 2019;11(13):12504–15.
[44] Zhai C, Zhu M, Bin D, Ren F, Wang C, Yang P, et al. Two dimensional MoS2/graphene composites as promising supports for Pt electrocatalysts towards methanol oxidation. J Power Sources 2015;275:483–8.
[45] Askari MB, Salarizadeh P. Ultra-small ReS2 nanoparticles hybridized with rGO as cathode and anode catalysts towards hydrogen evolution reaction and methanol electro-oxidation for DMFC in acidic and alkaline media. Synth Met 2019;256:116131.
[46] Feng L, Yao S, Zhao X, Yan L, Liu C, Xing W. Electrocatalytic properties of Pd/C catalyst for formic acid electrooxidation promoted by europium oxide. J Power Sources 2012;197:38–43.
[47] Zhang JJ, Sui XL, Zhao L, Zhang LM, Gu DM, Wang ZB. Hybrid of molybdenum trioxide and carbon as high performance platinum catalyst support for methanol electrooxidation. Int J Hydrogen Energy 2017;42(4):2045–53.
[48] Shi W, Park AH, Xu S, Yoo PJ, Kwon YU. Continuous and conformal thin TiO2-coating on carbon support makes Pd nanoparticles highly efficient and durable electrocatalyst. Appl Catal B Environ 2021;284(July 2020):119715.
[49] Wang K, Wang B, Chang J, Feng L, Xing W. Formic acid electrooxidation catalyzed by Pd/SmOx-C hybrid catalyst in fuel cells. Electrochim Acta 2014;150:329–36.
[50] Yang C, He H, Jiang Q, Liu X, Shah SP, Huang H, et al. Pd nanocrystals grown on MXene and reduced graphene oxide co-constructed three-dimensional nanoarchitectures for efficient formic acid oxidation reaction. Int J Hydrogen Energy 2021;46(1):589–98.
[51] Pramanick B, Kumar T, Halder A, Siril PF. Engineering the morphology of palladium nanostructures to tune their electrocatalytic activity in formic acid oxidation reactions. Nanoscale Adv 2020;2(12):5810–20.
[52] He N, Gong Y, Yang Y, Wang Y, Qin C, Wang R, et al. An effective Pd@Ni-B/C anode catalyst for electro-oxidation of formic acid. Int J Hydrogen Energy 2018;43(6):3216–22.
[53] Li R, Hao H, Huang T, Yu A. Electrodeposited Pd-MoO x catalysts with enhanced catalytic activity for formic acid electrooxidation. Electrochim Acta 2012;76:292–9.
[54] Salarizadeh P, Askari MB, Seifi M, Rozati SM. MoS2 coating on different carbonaceous materials: comparison of electrochemical properties and hydrogen evolution reaction performance. J Electroanal Chem 2019;847:113198.
[55] Chang J, Feng L, Liu C, Xing W, Hu X. An effective Pd-Ni2P/C anode catalyst for direct formic acid fuel cells. Angew Chem Int Ed 2014;53(1):122–6.
[56] Rodriguez JA, Jirsak T, Chaturvedi S. Reaction of S2 and SO2 with Pd/Rh(111) surfaces: effects of metal–metal bonding on sulfur poisoning. J Chem Phys 1999;110(6):3138–47.
[57] Yang Y, Wang G, Ge S, Yang H, Liu M, Liu M. Study on anti-sulfur dioxide poisoning of palladium-based catalyst for toluene catalytic combustion. Int J Hydrogen Energy 2021;46(9):6329–40.
[58] Obradović MD, Gojković SL. HCOOH oxidation on thin Pd layers on Au: self-poisoning by the subsequent reaction of the reaction product. Electrochim Acta 2013;88:384–9.
[59] Hossain SS. Bimetallic Pd–Fe supported on nitrogen-doped reduced graphene oxide as electrocatalyst for formic acid oxidation. Arabian J Sci Eng 2021;46(7):6543–56.
[60] Hong S, Kim H, Kim J, Kim SY, Ahn SH. Electrochemical synthesis of Pt-decorated Au dendrite anode for constructing a direct formic acid fuel cell. Mater Today Chem 2022;26.
[61] Lou M, Wang R, Yang L, Jia D, Sun Z, Wang L, et al. Ionic liquid polyoxometalate-enhanced Pd/N,P-codoped coal-based carbon fiber catalysts for formic acid electrooxidation. Appl Surf Sci 2020;516:146137.
[62] Yang Q, Lin H, Wang X, Zhang LY, Jing M, Yuan W, et al. Dynamically self-assembled adenine-mediated synthesis of pristine graphene-supported clean Pd nanoparticles with superior electrocatalytic performance toward formic acid oxidation. J Colloid Interface Sci 2022;613:515–23.